Aswan University Journal of Science and Technology Volume 4, issue 4

Optimizing of 5G Base Station MIMO Antenna Performance

Mai S. Abdel-Fattah[1,*], Tamer G. Abouelnaga[2], Ehab K. I. Hamad[3], Hala A. Elsadek[2]

[1] Communications Dept., Modern Academy for Engineering& Technology, Cairo, Egypt
[2] Microstrip Circuits Dept., Electronics Research Institute, Elnozha, Cairo 11843, Egypt
[3] Electrical Engineering Dept., Faculty of Engineering, Aswan University, Aswan 81542, Egypt

Abstract To improve 5G base station antenna performance, the study presents a novel dual-band high-gain four-port MIMO antenna with a frequency selective surface (FSS). The antenna resonates at 37.5 GHz (7.8% fractional bandwidth) and 3.5 GHz (53.3% fractional bandwidth), covering the sub-6 GHz and mmWave bands crucial for 5G. It has a straightforward monopole design with a cross slot and partial ground; it measures 82×76×1.524 mm³. Using frequency selective surface (FSS) for every band for beam steering, increases antenna gain, and isolation. Four different radiation patterns are displayed, with isolation levels of -15 dB and -34 dB and maximum gains of 8.5 dB and 11.2 dB. FSS is enhancing data rates and throughput for single or array antenna elements across both frequency ranges, which has been verified by practical experiments conducted with the FEKO-WinProp platform. Significant performance improvements are demonstrated by the results, which include a 25% increase in throughput (150 MB/s to 187.7 MB/s) and a 20% increase in data rate (1.5 MB/s to 1.8 MB/s) in the sub-6 band. With FSS implementation, data rates in the mmWave band increase by 72% (579.9 kB/s to 1.08 MB/s) and throughput increases by 62% (192 MB/s to 305.3 MB/s). There is also a noticeable increase in reference signal strength indicators (RSSI), indicating improvements in signal quality. The results show significant performance improvements, up to 200 % in data rate.

Keywords: 5G Base station, Sub-6 GHz, mmWave, Radio network planning, Wave propagation models

1. Introduction

The 5G wireless communications system has shown to be an effective solution that satisfies new requirements for data rate, access time, efficiency, and reliability. It also offers connectivity to a wide variety of devices. The patch antenna, a crucial component of the modern wireless communication system, has played a vital role in this advancement. Mainly, Microstrip patch antennas are less expensive, lighter, simpler to assemble, and more easily adapted to various wireless communication and mobile radio applications than traditional microwave antennas.

In 2017, frequency bands 3.3-3.6 GHz and 4.8-5 GHz bands (sub-6 band) were officially declared in China for indoor and outdoor 5G base stations. The sub-6 GHz band offers improved range and coverage and is compatible with the current infrastructure for older 4G wireless systems. Compared to earlier generations of wireless networks, which utilized the conventional sub-6 GHz spectrum, mm-Wave offers higher improvements over the sub-6 GHz frequency range regarding bandwidth and data throughput. However, noise power also has a greater impact at higher frequency bands. Therefore, directionally patterned high gain beam steerable antennas are practically necessary. Several nations have made the spectrum above 6 GHz public: the 24–29 GHz, 37–40 GHz, and 66–76 GHz bands. Generally, a higher gain antenna is required for the 5G new generation. So, array structures were suggested in many research studies to have a high-gain performance system [1]. However, this solution introduces a large structure size. Many techniques are used to enhance microstrip antenna gain, such as metamaterials [2], [3], [4] partial ground [5], shorting pins [6] and using frequency selective surface to enhance antenna gain and beam tilting while maintaining a compact size [7]. Single-frequency systems cannot meet the enormous demands of communication capacity because the available spectrum resources are limited now. So, additional needs for dual and multiband antennas are required. Many designs in the literature introduced dual-band antennas for compact base stations, which are presented in [8], [9], [10], [11]. These schemes introduced coupling between antenna elements and should be handled by decoupling techniques such as in [12], which uses a periodic structure between elements. In [13], a zigzag shape between the antennas is used, enlarging the base station antenna and adding more complexity.

Corresponding author E-mail: may.sameer@eng.modern-academy.edu.eg

Received September 28, 2024, received in revised form, October 6, 2024, accepted October 7, 2024.

(ASWJST 2021/ printed ISSN: 2735-3087 and on-line ISSN: 2735-3095) https://journals.aswu.edu.eg/stjournal

To guarantee standard performance and maintain the dependability of 5G systems, RF propagation models, including path loss models, must be developed. The deployment of 5G technology must handle massive data traffic and resolve connectivity problems to satisfy the demands of users with high connectivity and data rates.

It is anticipated that, due to the sustained increase in smartphone usage, global mobile data traffic will amount to approximately 130 Exabytes per month, four times more than that of 2019. Of this traffic, 35 percent will be carried by 5G networks [14] [15]. In higher frequency bands (24 GHz–40 GHz), individual cell site coverage will be approximately 100 m (in radius) instead of several kilometres in 4G networks. To guarantee end-user connectivity for the same area, the mobile network operator (MNO) must, therefore, install hundreds of new small cells (e.g., 100 m cell radius) as opposed to a single large cell site (e.g., Macrocell will have several km in radius). High levels of network availability and reliability, as well as 100% network coverage, are necessary for the 5G network [16]. Indicating that one of the (MNO) top priorities will be to plan the coverage of the 5G network. It guarantees connectivity and satisfies the 5G network Key Performance Indicator (KPI), including the lowest latencies and highest throughput and data rates and enhancing parameters, such as signal interference noise ratio (SINR), reference signal reception power (RSRP), and reference signal reception quality (RSRQ). As RSRP is the amount of received power by user equipment based on the distance between the cell and user equipment when it is small, it means there is a need for a handover process; RSRQ is defined as received signal quality measurement from the cell it is the ratio between the number of RSRP resource blocks to RSSI (Received Signal Strength Indicator), SINR is the ratio of the power of received signal to the interference power and noise power received by the user.

Numerous studies have examined network coverage performance from various angles in [17]. It assumes the 2x2 MIMO element antenna that maximum data rate reached is 2M B/s still small, so for bitrate enhancement, it suggests an increased number of MIMO elements to be 8x8 that increase bit rate that reaches max 3MB/s. Enhancement could be made by modifying base station antenna performance to enhance network capacity and coverage, hence bit rate and throughput enhancement.

This paper presents antenna designs with a high gain and dual-frequency spectrum, enhancing their performance using a frequency-selective surface (FSS) added to the antenna at both frequency bands. Although adding FSS introduces a larger volume, but the antenna is still compact and cost-effective because of using a low-cost substrate. Also, it is simple, and MIMO has high isolation without adding isolation techniques. It is applied to the real world using Winprop software, which enhances the network coverage for both bands using the antenna with FSS. Results show enhancement in data rates and throughput and also for reference signals.

Power analyses are also studied to show modified antenna performance under different environmental circumstances, showing loss and attenuation effects over signal travelling from transmitter to receiver. These findings are based on the requirements for base station 5G antennas. Maximum data rates of 3.08 MB/s by 64-QAM modulation with Extended-Walfisch propagation model using 2x2 MIMO elements with FSS and SNIR, reference signals (RSRP-RSRQ-RSSI) are also analyzed, network coverage done with three sites having each three sectors once using single and 2X2 MIMO antenna and again with the modified antenna plus FSS in sub-6 and mm-wave bands.

2. Antenna Design and Simulations

2.1. The proposed single-element antenna

The design aims to group antennas with more than one function for different mobile operators, thus conserving tower space and making maintenance easier. Here, the antenna operating at 2.2-3.8 GHz and 35.6-38.5 GHz bands are chosen for the 5G base station. Figure 1 shows the top and back perspectives of the dual-band proposed antenna's 2D configuration. The 50 Ω microstrip line is positioned on a 37 ×41 mm^2 Rogers RO3003 substrate with a thickness of 1.524 mm and a relative dielectric constant of 3. The ground is etched with different rectangular slots to reduce the antenna's electrical size. The proposed antenna is combined with the proposed FSS, which operates in two various frequency bands to enhance the antenna's performance. Table 1 lists the optimized parameters for the proposed antenna.

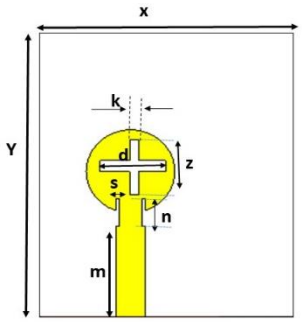

(a)

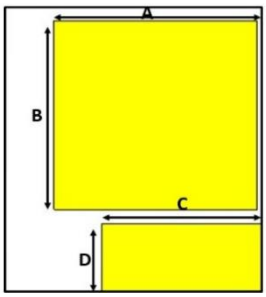

(b)

Figure 1. Proposed single-element antenna, (a) front view and (b) Back view

Table 1. Optimized dimensions of the proposed antenna in mm

Par.	*Value (mm)*	*Par.*	*Value (mm)*
X	41	s	0.5
Y	35	m	13
z	8	n	4
d	8.4	A	28.5
B	27	*C*	22
D	10	k	1.2

2.2. Proposed FSS unit cell design

Enhancing antenna parameters represents a pivotal aim for base station antennas, necessitating the utilization of Frequency Selective Surfaces (FSS) to enhance dual-band sub-6 GHz and mm-wave band performance.

Figure 2(a) shows the schematic diagram of the proposed low-frequency FSS unit cell for the sub-6 GHz band and its optimized parameters. It comprises a square ring of 13.2×13.2 mm2 and is printed on an FR-4 substrate with a thickness of 1.6 mm and a dielectric constant ε_r of 4.3 with 0.025 a loss tangent. Its equivalent (*LC*) circuit model consists of three series inductors $L_1 = L_2 = L_3$ = 0.1 nH connected with a parallel capacitor of C_1 = 2.6 pf, as shown in Fig. 2(b). In Fig. 2(c), transmission coefficients for the unit cell and its response at the low-frequency band indicate that the cells have a reflection response to reject a band around 4 GHz. In CST software, the transmission coefficients are computed with a periodic boundary condition.

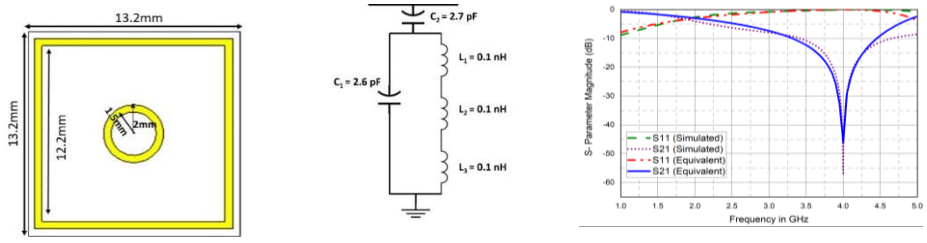

(a) (b) (c)

Figure 2. FSS unit cell for sub-6 band, (a) Unit cell structure and (b) Its equivalent circuit, (c) The simulated EM and from its equivalent circuit S-Parameters

Figure 3(a) shows the schematic view of the proposed High-frequency FSS unit cell for the mm-wave band and its geometrical configuration parameters. It comprises a square ring 2.6×2.6 mm^2 printed on the front side of Roger RO3003 substrate with a thickness of 1.524 mm, a dielectric constant εr of 0.3, and loss tangent tan δ of 0. 001. The Equivalent circuit model at 37 GHz consists of a capacitor of 0.025 pF in parallel with three inductors of 0.03 nH, shown in Fig. 3(b). The S parameters of the proposed equivalent circuit contrasted with the identical result in CST are shown in Fig. 3(c). Both results are matched well at the resonance frequency of 37 GHz.

The main goal of adding FSS is to improve the gain and antenna beam to redirect direction. antenna's at sub-6 the desired broadside The radiation while the GHz is band is radiation, so using mm-wave for both end-fire, not be one FSS acceptable. Thus, the FSS proposed structure is expected to differ in the two-frequency spectrum, as illustrated in Fig. 4. The proposed low-frequency FSS (sub-6G) is placed in the back of the proposed antenna (parallel to the antenna). The high-frequency FSS (mm-wave) is placed as a side wall of the antenna (perpendicular to the antenna). The high-frequency FSS dimensions are 21.2×36.7 mm^2, while the low-frequency FSS dimensions are 98.4×98.4 mm^2, placed at j=20 mm apart from the backside of the proposed antenna. The FSS on the backside of the proposed antenna reflect the backside radiation and enhances the front-to-back ratio (F/B) of the developed MIMO antenna.

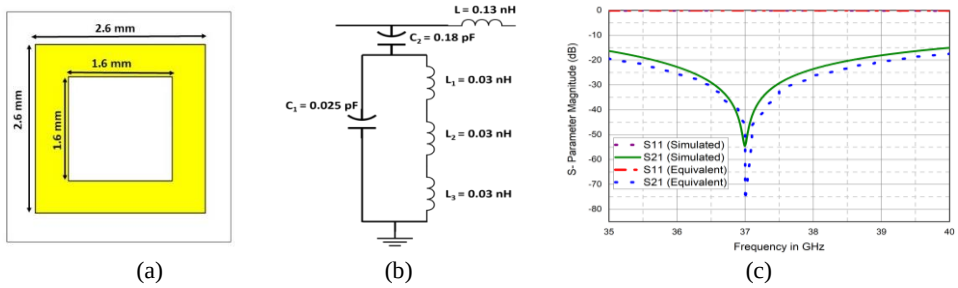

(a) (b) (c)

Figure 3. FSS unit cell for the mm-wave band, (a) Unit cell structure and (b) its Equivalent circuit, (c) Simulated S-parameters, EM, and from circuit modelling

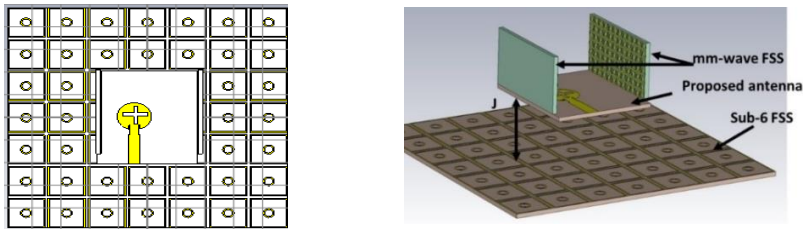

(a) (b)

Figure 4. Proposed single element with FSS (a) front view and (b) side view

The design and simulations of the proposed antenna are carried out using the CST Microwave Studio 2019 simulator. The reflection coefficients of the proposed antenna with and without the FSS unit cells at the sub-6 GHz and mm-wave bands are illustrated in Figures 5 (a) and (b).

The antenna gain enhances from 4 dB to 9.1 at GHz and sub-6 to 11 dB from 9.8 mm- at the band wave as depicted in Fig. 5(c), (d), and the main beam is steered to the front side and beam width reduced that allow more directive radiation as shown in Fig. 6.

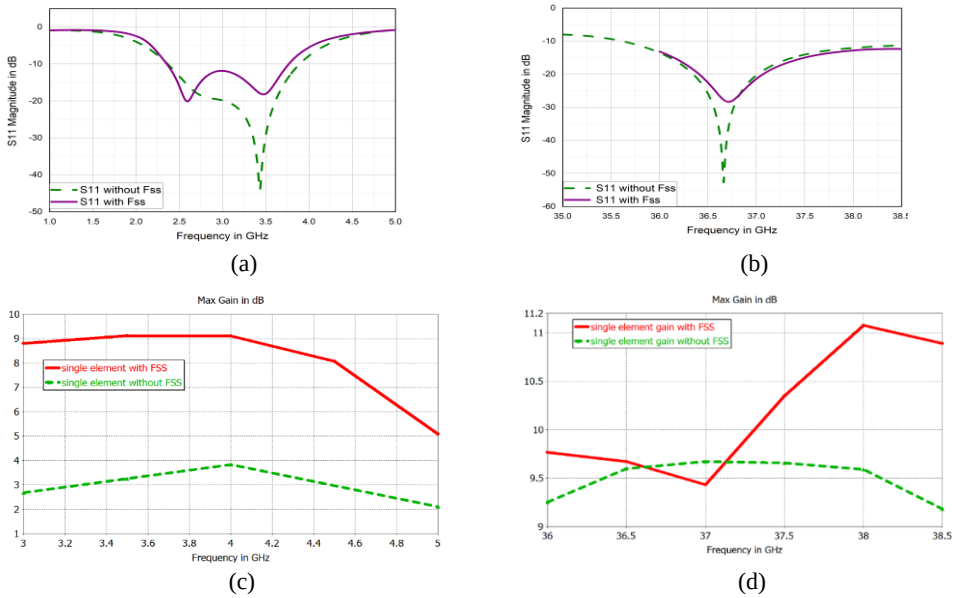

(a) (b) (c) (d)

Figure 5. Simulated reflection coefficients of the proposed antenna (a) with FSS for sub-6 GHz band, (b) without FSS for mm-wave band, The gain of the antenna at (c) sub-6 GHz band with FSS and (d) mm-wave bands without FSS.

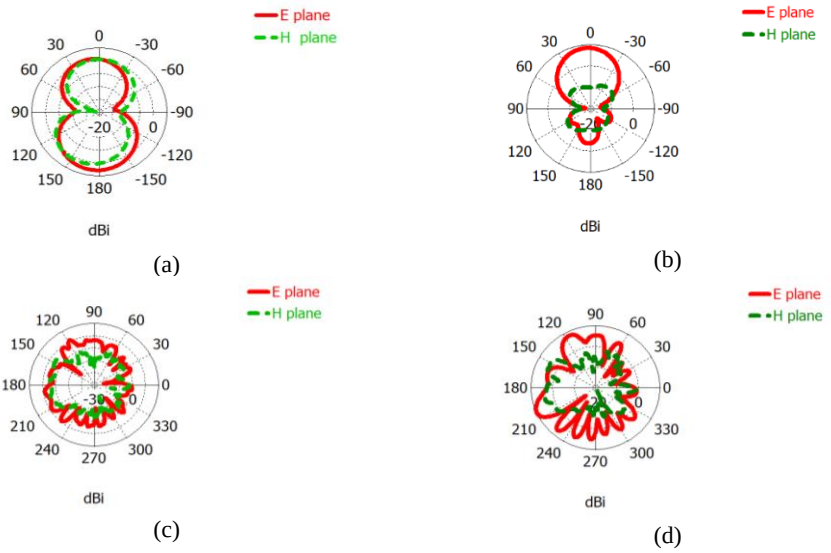

Figure 6. E-plane and H-plane polar radiation pattern at sub-6 (a) without FSS,(b) with FSS ,(c), (d) mm-wave band

We may use different structures of FSS that will affect the main antenna performance. Still, this proposed design gives better gain, directivity and bandwidth results with low cost and easily fabricated design.

3. MIMO Antenna Design Structures

3.1. Four- MIMO antenna.

The proposed four-element MIMO antenna elements are placed orthogonally to each other on a substrate of 82×76×1.524 mm^3, as indicated in Fig. 7(a). The internal element spacing is 47.3×53.3 mm^2, the minimum distance that can be set without ground overlapping. The frequency selective surface used for both bands is shown in Fig. 7(a), one underneath the 4-element MIMO for the sub-6 GHz band at a distance of 20 mm and the other on the sides of each of the four elements for the mm-wave band with a height of 21.2 mm.

Figure 7. Proposed four-elements MIMO antenna, (a) perspective, (b) top view

The reflection and transmission coefficient values for the sub-6 band MIMO antenna are illustrated in Fig. 8. a 2.3 GHz to 3.8 GHz impedance bandwidth with S_{11} -27.8 dB and a maximum gain of 8.7 dB is achieved. The mutual coupling effect between MIMO elements is about -16.6 dB between antenna 1 and 3 and -54 dB between 1 and 2. At the mm-wave band in Fig. 8(b), the 4-element MIMO introduces a large bandwidth of 3 GHz and a maximum gain of 11.2dB shown in Fig. 8. c, d. The minimum isolation between antennas 3 and 2 is about -34.5 dB, while a maximum isolation of -62.4 dB is between antennas 3 and 4. Many parameters are used to analyze the MIMO antenna's performance. The envelope correlation coefficient (*ECC*) is one of the key essential characteristics determining the MIMO's performance. The diversity gain (*DG*) is calculated for the antenna and is estimated using the *ECC*.

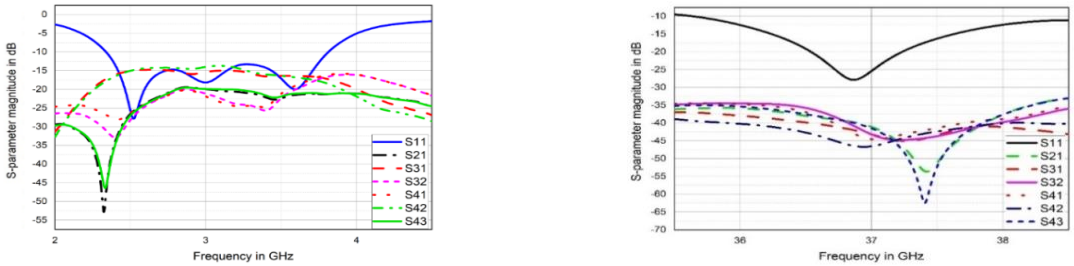

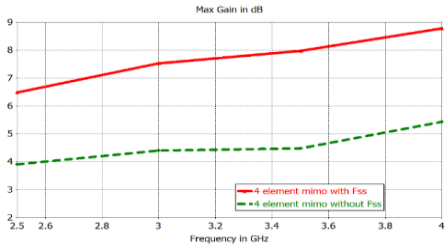

(c)

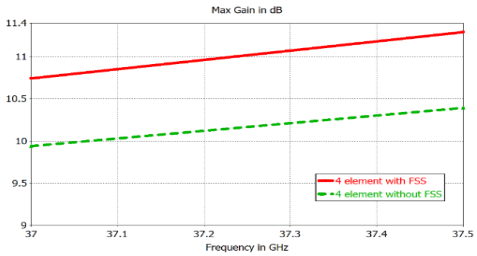

(d)

Figure 8. Reflection and transmission coefficients of four elements MIMO at (a) sub-6 GHz band, (b) mm-wave band, and the gain of proposed four elements MIMO: (c) with FSS, (d) without FSS

3.2. Performance Analysis of MIMO antenna.

This section discusses and analyzes the critical parameters of the four-port MIMO antenna. The diversity gain (DG) and the envelope correlation coefficient (ECC) are vital parameters in the MIMO systems [19, 20]. The correlation between the elements of the MIMO configuration is known as the ECC. Higher MIMO performance is achieved when there is less ECC between the MIMO elements; this value can be calculated from the radiation pattern as presented in [18]

$$ECC = \rho_{ij} = \frac{\left|\iint_0^{4\pi}\left[\overrightarrow{F1}(\vartheta,\varphi) * \overrightarrow{F2}(\vartheta,\varphi)\right]d\Omega\right|^2}{\iint_0^{4\pi}\left|\overrightarrow{F1}(\vartheta,\varphi)\right|^2 d\Omega + \iint_0^{4\pi}\left|\overrightarrow{F2}(\vartheta,\varphi)\right|^2 d\Omega} \quad (1)$$

where $\overrightarrow{F1}(\vartheta,\varphi)$ and $\overrightarrow{F2}(\vartheta,\varphi)$ represent the 3D radiation patterns of Ant. 1 and Ant. 2, respectively, while Ω is the solid angle. The acceptable limit of the ECC should be lower than 0.5. The low value of the ECC guarantees good isolation between the radiating elements. As illustrated in Fig. 9 (a, b), the simulated value of ECC is below 0.015 and 0.00014 over the sub-6 and mm-wave bands, respectively.

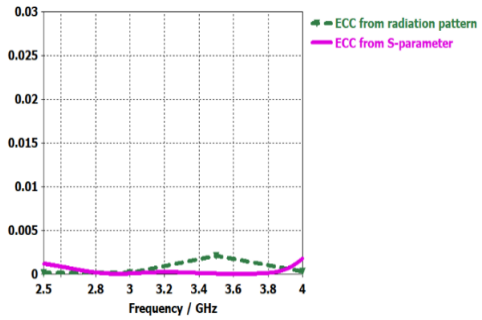

(a)

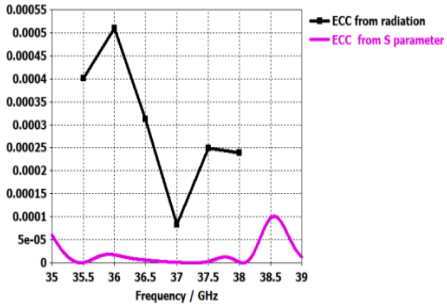

(b)

Figure 9. Simulated ECC for (a) sub-6G (b) mmWave frequency spectrum.

Another approach to characterizing and assessing the proposed 2×2 MIMO antenna configuration's effectiveness is Diversity Gain (DG), which quantifies transmission power degradation. DG can be computed utilizing the ECC of the MIMO antenna according to the following equation [19]**.** Figure 10 shows the DG of the simulated 4-element MIMO for both sub-6 GHz and mm-wave bands, which shows a best value of 10 within the desired band.

$$DG = 10\sqrt{1 - (ECC)^2} \quad (2)$$

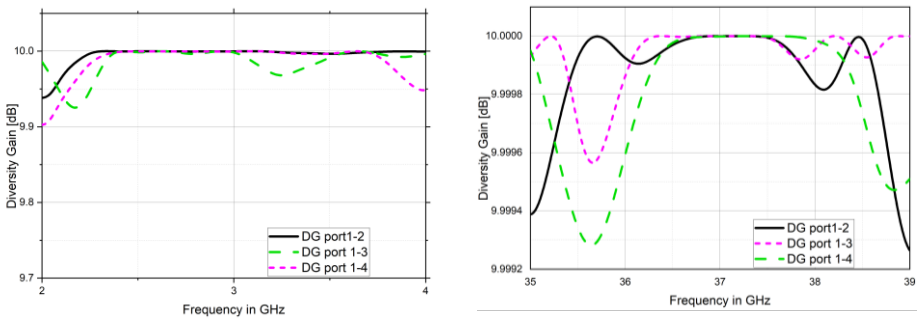

(a) (b)

Fig. 10. DG for the proposed 4-element MIMO antenna for (a) sub-6G and (b) mm-wave bands.

The radiation performance of the MIMO antenna is represented by the total active reflection coefficient (TARC). TARC is the ratio of the square root of total reflected power divided by the square root of total incident power. It can be calculated using the following relation.

$$TARC = \sqrt{\frac{|S_{11}+S_{12}e^{j\theta}+S_{13}e^{j\theta}+S_{14}e^{j\theta}|^2+|S_{21}+S_{22}e^{j\theta}+S_{23}e^{j\theta}+S_{24}e^{j\theta}|^2+|S_{31}+S_{32}e^{j\theta}+S_{33}e^{j\theta}+S_{34}e^{j\theta}|^2+|S_{41}+S_{42}e^{j\theta}+S_{43}e^{j\theta}+S_{44}e^{j\theta}|^2}{2}} \quad (3)$$

The practical value of TARC always lies between 0 and 1, which means less than 0 dB. Figure 11 (a, b) shows TARC variation versus frequency of the two proposed frequency spectrums: the sub-6 band and the mm-wave band, and it is observed that it is mostly less than -5 dB. Consequently, the lower ECC value suggests that the recommended 4-port MIMO system offers a superior diversity pattern.

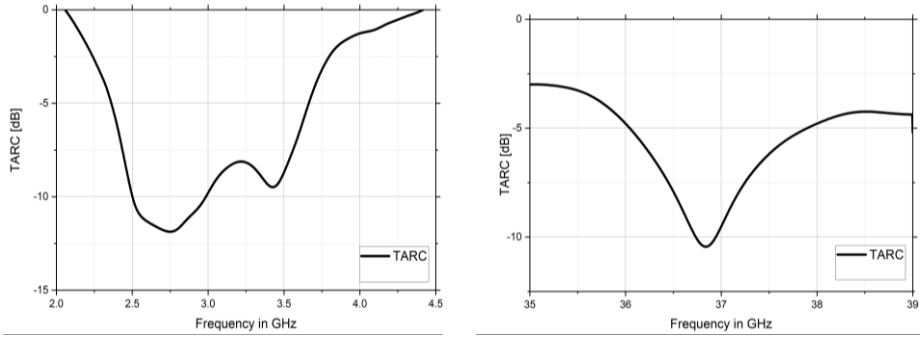

Figure 11 TARC variation versus frequency at (a) sub-6G band (b)mm-wave band

4. Network Coverage enhancing

Modified antennas are tested in real-world using Winprop software and the air interface model suitable for each band with Extended Walfisch-Ikegami model (EWM) as a propagation model having small run time compared to its accuracy; results are calculated for both single element and 2x2 MIMO antenna without FSS in base station located at Frankfurt as deployed area, three sites each have three sector antenna (0^o,120^o,240^o). Results indicate lower data rates and throughput unsuitable for 5G requirements. Adding FSS to single elements or MIMO enhances data rates and throughput as 5G technology aims to significantly improve data rates and throughput compared to previous generations of wireless networks.

Max data rate and throughput for single element working at sub-6 enhanced from 1.5 MB/s to 1.8 MB/s by 20% and 150 MB/s to 187.7 MB/s by 25%, respectively, in DL (Down Link)and UL(Up Link) when using FSS underneath the antenna and enhanced by 72% from 579.9 kB/s to 1.08 MB/s and throughput from 192 MB/s to 305.3 MB/s by 62% in mmWave frequency band when using FSS on single element's sides. Reference signal also enhanced in sub-6 RSSI from -54 dBm to -45 dBm (83%), and in mm-wave, it was -64 dBm reached -50 dBm when using FSS. To achieve high data rates and large capacity, the 5G network is integrated with small cells, MIMO, beam-forming, and mm Waves. So 2x2 MIMO elements are tested and also enhanced in sub-6, data rate and throughput 173.7KB/s to 1.4 MB/s (800%), 17.3 MB/s to 200.8 MB/s (116%) respectively in DL and also in UL it increases from 22.7 kB/s to 1.5 MB/s (660%), 2.2 MB/s to 214.8 MB/s (972%) at mm-wave data rate and throughput 2.9MB/s to 3.08MB/s (6%),

780.9 MB/s to 814.2 MB/s (4%), respectively in DL and also in UL, it increases from 3.1 MB/s to 3.29 MB/s (6%), 835.4 MB/s to 871 MB/s (4%)

The simulation results show that the signal strength is excellent. Also, the minimum transmitter power for the base station is 45dBm, which is suitable for the requirements suggested by 3GPP [20].

Table 2. Results comparing single element antenna with and without FSS

Single element	Sub-6 No FSS	Sub-6 With FSS	mm-wave No FSS	mm-wave with FSS
DL (max data rate)	1.5 MB/s	1.8 MB/s	579.9 kB/s	1.8 MB/s
Throughput	150 MB/s	187.7 MB/s	179.5 MB/s	285.4 MB/s
UL (max data rate)	1.5 MB/s	1.8 MB/s	727.3 kB/s	1.15 MB/s
Throughput	150 MB/s	187.7 MB/s	192 MB/s	305.3 MB/s
RSRP	-90 dBm	-80 dBm	-94 dBm	-80 dBm
RSRQ	-11.5 dB	-11 dB	-5 dB	-5 dB
RSSI	-54 dBm	-45 dBm	-64 dBm	-50 dBm

Table 3. Results comparing 2×2 MIMO elements with and without FSS

2×2 MIMO element	Sub-6 No FSS	Sub-6 With FSS	mm-wave No FSS	mm-wave with FSS
DL (max data rate)	173.7 kB/s	1.4 MB/s	2.9 MB/s	3.08 MB/s
Throughput	17.3 MB/s	200.8 MB/s	780.9 MB/s	814.2 MB/s
UL (max data rate)	22.7 kB/s	1.5 MB/s	3.1 MB/s	3.29 MB/s
Throughput	2.2 MB/s	214.8 MB/s	835.4 MB/s	871MB/s
RSRP	-70 dBm	-60 dBm	-40 dBm	-70 dBm
RSRQ	-12 dB	-5 dB	-5 dB	-4 dB
RSSI	-35 dBm	-30 dBm	-10 dBm	-35 dBm

This section shows RF signal tracing and real-world 5G network coverage simulation, with Frankfurt as the deployment area Using Winprop software.

Here is a comparison that shows the coverage area enhancement using FSS for sub-6 and mm-wave either in a single element or 2x2 elements MIMO using three sites, each having three sector antenna at (0^o,120^o,240^o) using Extended Walfisch-Ikegami Model as it has the shortest run time compared to its accuracy.

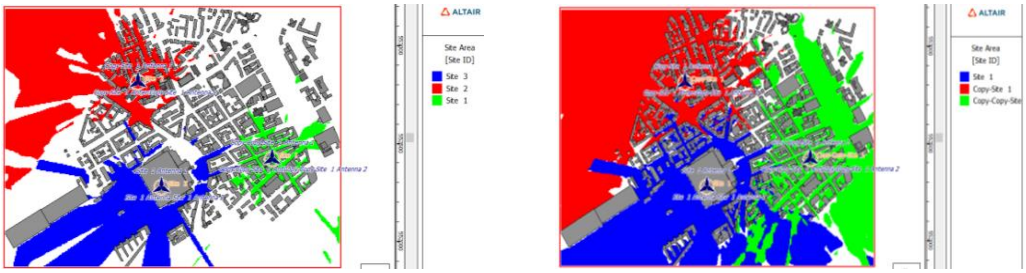

Figure 12 Coverage for the single element at sub-6; (a) without FSS; (b) with FSS

Figure 12 shows three sectors with a single three-element antenna, each has a colour representing its coverage area; at the sub-6 band without FSS in (a) small area can be covered and enhanced in (b) as using FSS with the single element. Also, figure 13 shows single element at mm-wave, a higher frequency band antenna covers a smaller area that can be modified using FSS in (b).

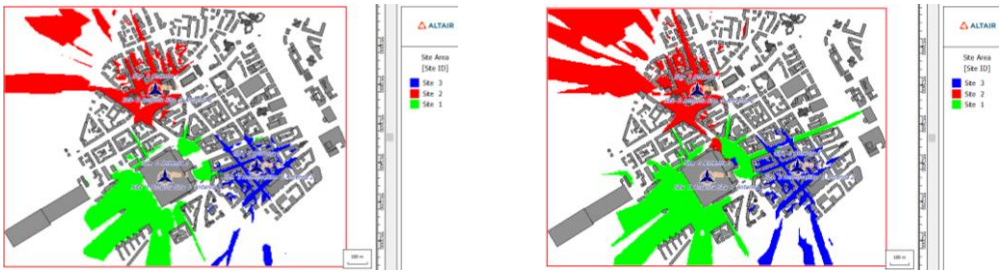

Figure 13 Coverage for the single element at mm-wave (a) without FSS (b) with F

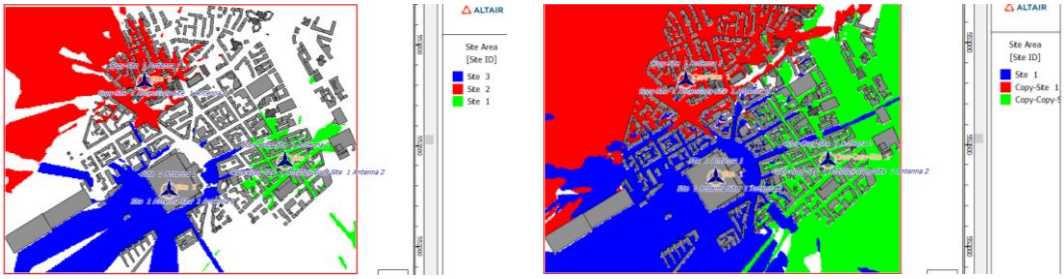

Figure 14 Coverage for the 2x2-MIMO element at sub-6 (a) without FSS (b) with FSS

As shown in Figure 14, instead of using a single element, we use 2x2 element MIMO to enhance data rates, but in (a) still, the coverage area is small; applying FSS in (b), the coverage area improves, and almost all areas around the antenna are served. The area covered in figure 15 is small as the antenna operates at a higher frequency band, but it improves in (b) using FSS

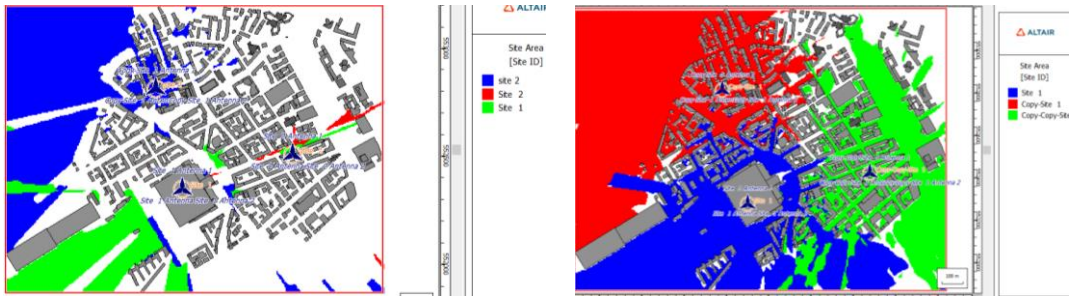

Figure 15 Coverage for 2×2 MIMO element at mm-wave (a) without FSS (b) with FSS

Without using FSS, three sector antennas cannot cover all areas around them, as seen in Figs. 12,13,14,15, but adding FSS enhance coverage area, and almost all areas around the base station can serve users in this area.

5. Power analysis of the proposed antenna.

5.1 Free space path loss

The signal propagation loss is excessively increased in high-frequency bands, drastically decreasing each cell site's coverage. In higher frequency bands (i.e., 24GHz–40GHz), individual coverage of cell sites will be approximately 100 meters (radius) [16] rather than a few kilometres at 4G networks. So, the mobile network operator (MNO) must launch hundreds of new tiny cells. Instead of one sizeable macro cell to guarantee end users' connectivity for the same area.

$$\boldsymbol{L} = \left(\frac{\boldsymbol{\lambda}}{\boldsymbol{4\pi d}}\right)^{\boldsymbol{2}} \qquad (4)$$

where λ is free space wavelength, d is the distance between the transmitter and receiver. Free space path loss simulation versus operating frequency up to 100 GHz, including sub-6 and mm-wave band frequency (3.5 and 37 GHz) shown in Fig. 16.

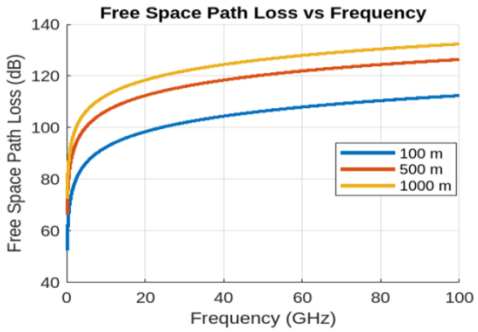

Figure 16. Path loss versus frequency at three different distances

It shows the variation of path loss at different-distance separation (100-500-1000m) between transmitter and receiver, as shown in table (4), path loss at the two operating frequencies of sub-6 and mm-wave for the proposed antenna.

Table 4. Path loss over distances (100-500-1000 m) for 3.5 and 37 GHz

Distance (m)	Frequency (GHz)	Path loss (dB)
100	3.5	83.32
	37	103.8
500	3.5	97.3
	37	117.7
1000	3.5	103.3
	37	123.8

It is discovered that the total signal attenuation arsis as the working frequency increases or if the propagation path increases. Hence, the 5G networks limit the cell range to 100 m for high-frequency bands. Many parameters affect the path loss, such as operating frequency, the distance between the base station, user equipment, the height of the antenna's site, and its nature (urban-rural-indoor). Also, system bandwidth allows high data rates but introduces more interference. Another parameter that affects signal attenuation is atmospheric conditions such as rainfall. Figure 13 shows the frequency variation up to 100 GHz versus signal attenuation at different rainfall rates.

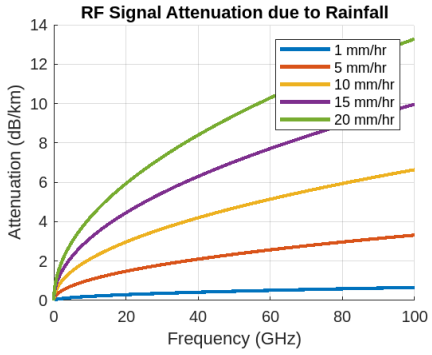

Figure 17. Attenuation due to rainfall versus frequency at different rain rates

Table 5 shows the attenuation of propagation signal at different rainfall rates at the two operating frequency bands (3.5, 37 GHz); results show high attenuation occurs in high rain rates or high frequency because of high absorption in high-frequency ranges.

Table 5. Attenuation at 3.5 and 37 GHz over different rain rates

rain rate (mm/hr)	attenuation at freq. 37 GHz in dB	attenuation at freq. 3.5 GHz in dB
1	-4.2	-29.3
5	1.9	-19.4
10	4.6	-15.2
15	6.2	-12.7
20	7.3	-10.9

5.2 RF link budget

The path loss was tested in three environments (hotspot indoor –dense and rural). Figure 18 shows the variation of path loss versus distance (0-20m) between transmitter and receiver at the hotspot indoor environment for sub-6 and mm-wave bands using the proposed antenna that had a gain of 11dBi for single element antenna for base station and 5dBi for mobile handset and path loss increased little bit at the mm-wave (40 dB). The test was done with 256 elements in the base station and eight elements in the mobile handset, as recommended in International Mobile Telecommunications (IMT-2020). As seen from results at hotspots indoor environment, 37 GHz introduces more losses that can be controlled using a higher gain antenna (nearly 5dBi more)

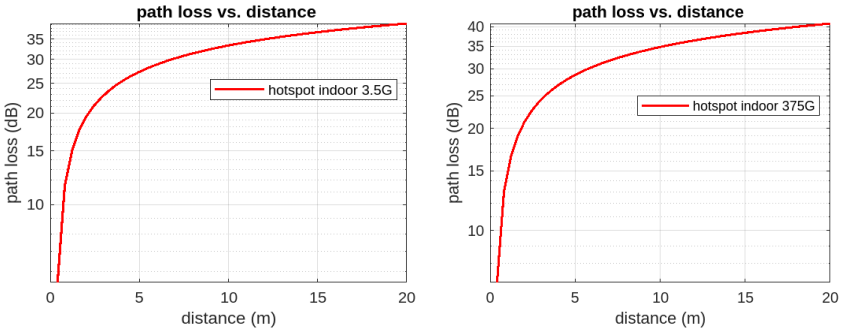

Figure 18. Path loss versus distance in Hotspot indoor environment (a) sub-6 (b) mm-wave

Figure 18 shows path loss in the dense environment at sub-6 (3.5 GHz) and mm-wave (37 GHz). The path loss increased at the mm-wave band by 15dB over the sub-6 band at the max cell radius of 200m, and it is expected in high frequency as it is sensitive to environmental parameters (tree-buildings). Still, the proposed antenna could work efficiently even in rural areas with a cell radius of up to 1700 m.

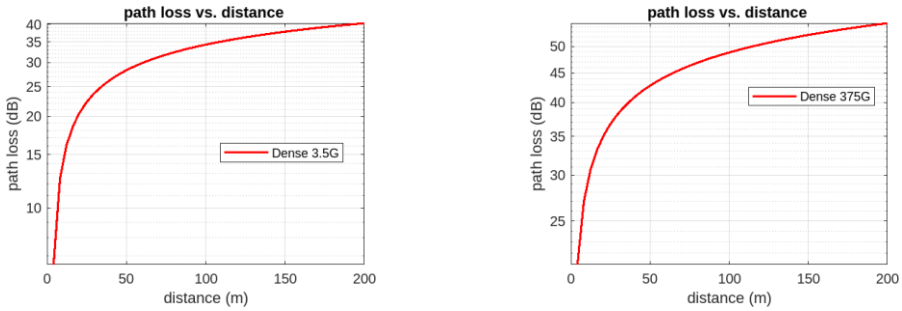

Figure 19 Path loss versus distance in a Dense environment

Figure 19 shows the effect of distance on the path loss at the sub-6 band, and path loss reaches a max level of 60dB at the highest distance of 1700 m

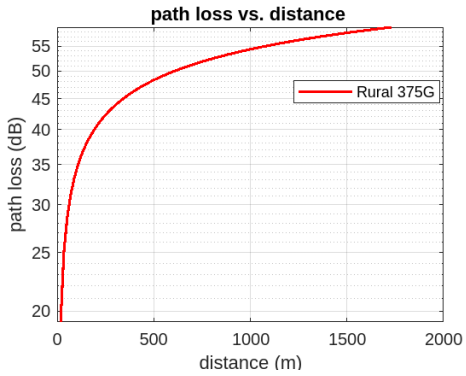

Figure 20. Path loss versus distance in Rural environment

5.3 SNIR in three different environments

Signal to Noise plus Interference Ratio SNIR (RSRP/RSRQ must be detected at a minimum of 20 dB). It displays the channel's throughput capacity and the usual range of values ≥ 20dBm (excellent), 13dBm to 20dBm (good), 0dBm to 13dBm (fair to poor), and ≤ 0dBm (no Signal/disconnection).

The tables below introduce MATLAB calculation for SINR at three different environments (rural- dense- hotspot) using equation 5

SINR = ((received power) /10×log10 ((total Interference Power + total Noise Power))) (5)

Noise Power = -174 dBm/Hz, interference Power = -90 dBm as defined in 3 GPP.

Results show received power in all cases larger than the minimum receiver sensitivity required (-90 dBm) as in [21].

SINR in the rural environment 3.5G	*30.33dB*
Rx power	*-25.34 dBm*
Noise Power:	*7.96e-14 Watts*
Interference Power:	*0.00 Watts*
SINR at Dense environment 3.5G	*30.33 dB*
Rx power	*-25.34 dBm*
Noise Power:	*7.96e-14 Watts*
Interference Power:	*0.00 Watts*
SINR at Dense environment 37G	*78.8 dB*
Rx power	*-65.83 dBm*
Noise Power:	*1.59e-13 Watts*
Interference Power:	*0.00 Watts*

SINR at hotspot environment 37G	*54.70 dB*
Rx power	*-45.83 dBm*
Noise Power:	*1.5e-13 Watts*
Interference Power:	*0.00 Watts*

SINR at hotspot environment 3.5G	*30.33 dB*
Rx power	*-25.34 dBm*
Noise Power:	*7.96e-14 Watts*
Interference Power:	*0.00 Watts*

6. Fabrication and Measurements

Proposed antenna measurements and construction are crucial steps in confirming the validity of the computational calculations. Photolithography is used to create the suggested antenna, and a vector network analyzer (VNA Rohde & Schwarz "ZVB20") is utilized for measurements. Figure 21 shows the antenna photos of the proposed prototype antenna with FSS for each band. It can be noticed from Fig. 22 that S_{11} are below -10 dB from 2.5 GHz to 4 GHz with and without FSS with an impedance bandwidth of 46% and from 35.5 to 37.5 with FSS and without FSS with an impedance bandwidth of 6.8% based on the measured results. Minor differences between the measured and simulated results are due to poor soldering, manufacturing tolerance, etc. A prototype of a 4-element MIMO antenna is fabricated, as shown in Fig. 23(a). Four walls of FSS printed on Roger substrate beside the antenna work to enhance radiation parameters for the high-frequency band, and FSS below the antenna works on the sub 6G band. Figure 23(c) shows the proposed 4-element MIMO front and back views that show the same partial ground as in single-element.

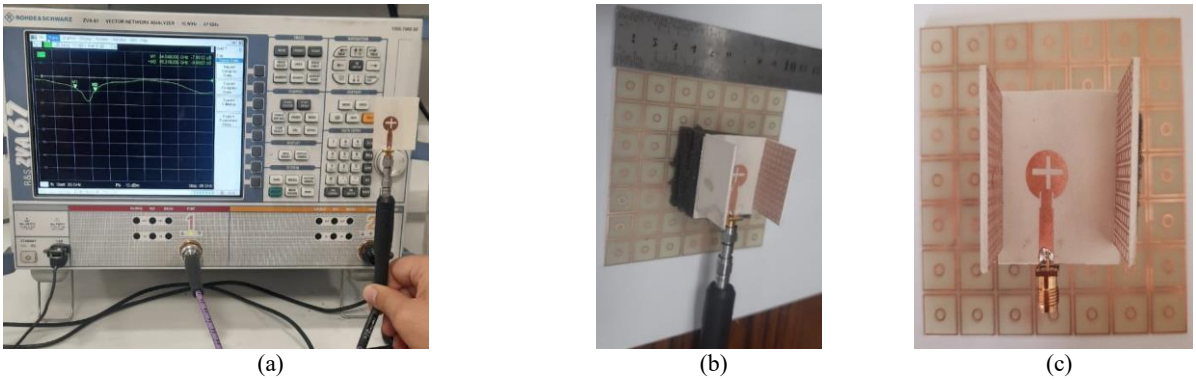

(a) (b) (c)

Figure 21 (a) Single patch with VNA (b) single patch with the two FSS (c) front view

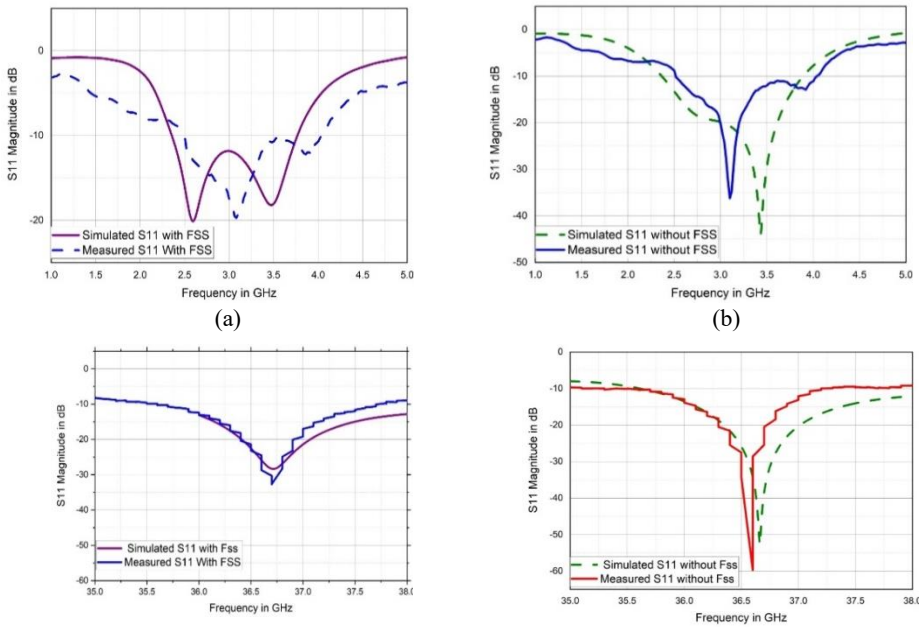

Figure 22 Simulated and measured S-parameters of the proposed antenna with and without FSS (a), (b) for low frequency (c), (d) for high frequency.

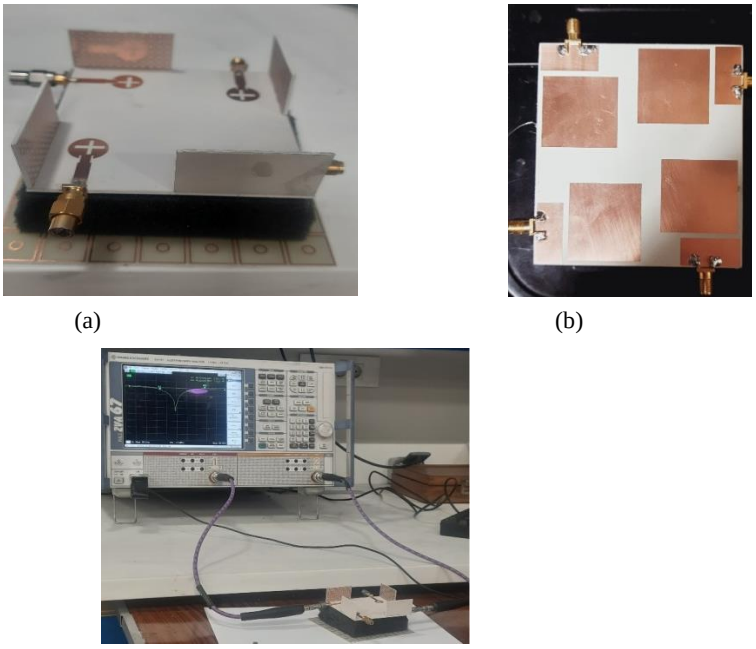

Figure 23. (a) (b) Front and back view of 4 elements MIMO (c) VNA during measure

Figure 24(a, b) displays the simulated and measured reflection and transmission coefficients of the 4-element MIMO antenna with FSS and Fig. (c, d) without FSS at sub 6G band. Orthogonal polarization is achieved when two linearly polarized waves are perpendicular to each other. The waves do not interact with each other, as they are orthogonally positioned. It is observed that there is a good agreement between the simulated and measured results. The measured impedance bandwidth is 40 % (2.4- 3.6 GHz). The measured isolation is better than -16 dB. However, Fig. 25 shows the simulated and measured results for the proposed 4-element MIMO at mm-Wave band, and it indicates a measured impedance bandwidth of more than 13% (35- 39 GHz) and isolation of better than 35 dB.

There is a tiny variation in the resonating point of this MIMO antenna design. The feed points are the leading cause of the notable differences between the simulated and measured results for particular operating bands. The measurements are significantly impacted because of the loss of the SMA connector. However, the resonator's bandwidth is almost the same in both scenarios. Significant variation is seen in the measured and simulated results for these MIMO antennas, which the influence of the soldering materials can partially explain. The connectors used in the measurement set may also be the reason for the change in either result. This difference could be caused by the antenna or the connector's impedance. The radiation pattern of simulated and measured results for the proposed single-element antenna in the *H* plane (x-y) and *E* plane (x-z) at 2.3 GHz are shown in Fig. 26.

According to the results, adding FSS underneath the patch and on each side of the patch steered the radiation pattern to the broadside direction. It was also found that the simulated radiation patterns agreed with the measured ones. The proposed antenna exhibited an omnidirectional radiation pattern. It was found that the simulated radiation patterns agree with the measured ones. The proposed antenna exhibited an omnidirectional radiation pattern.

All measurement processes have been carried out in the Center of Scientific and Technological Excellence, Cairo, Egypt, with the help of a 2D Anechoic Chamber as visualized in Fig. 27. The horn antennas performed as a transmitter surrounding the proposed antenna and are competent to function from 1 GHz to 18 GHz. The antenna being tested (single-element antenna) executes as a receiver.

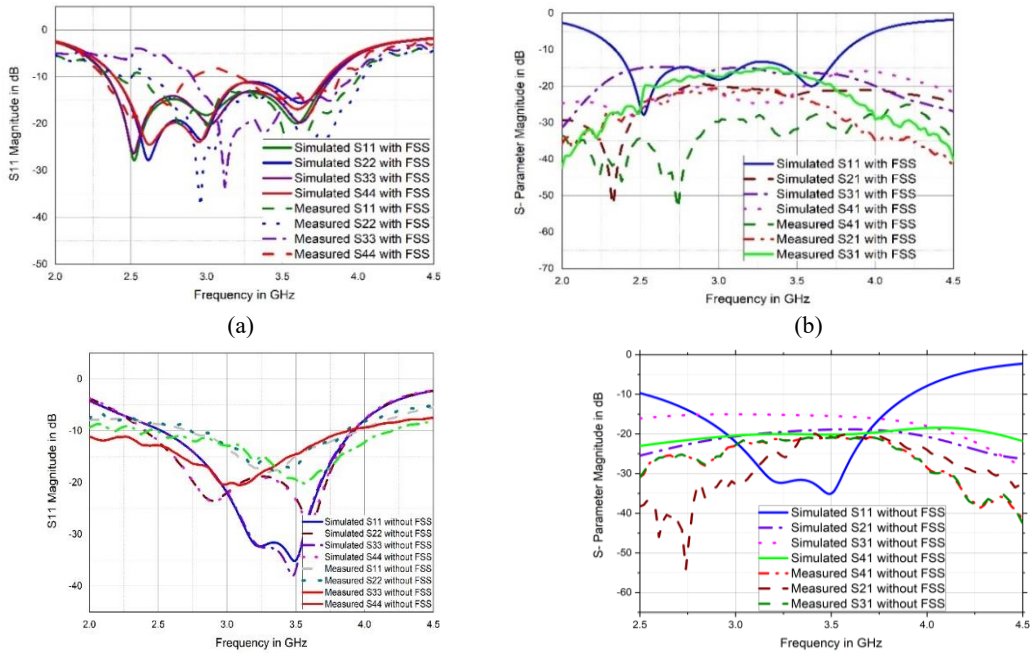

Figure 24. Simulated and measured S-parameter of proposed MIMO antenna at sub-6 GHz band (a), (b) with FSS, (c), (d) without FSS.

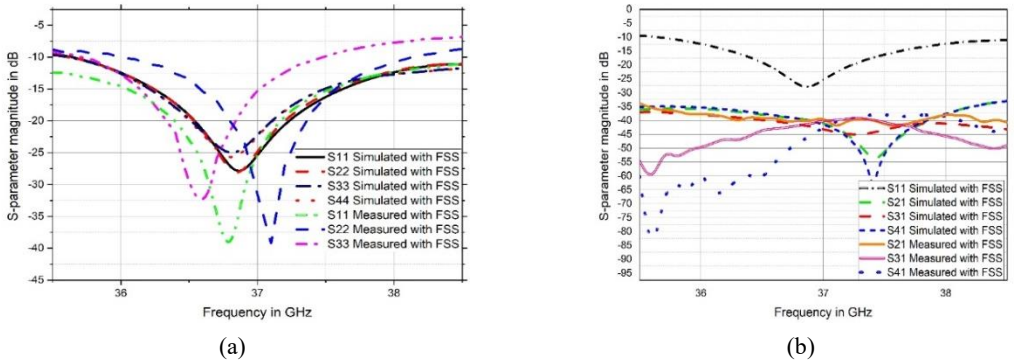

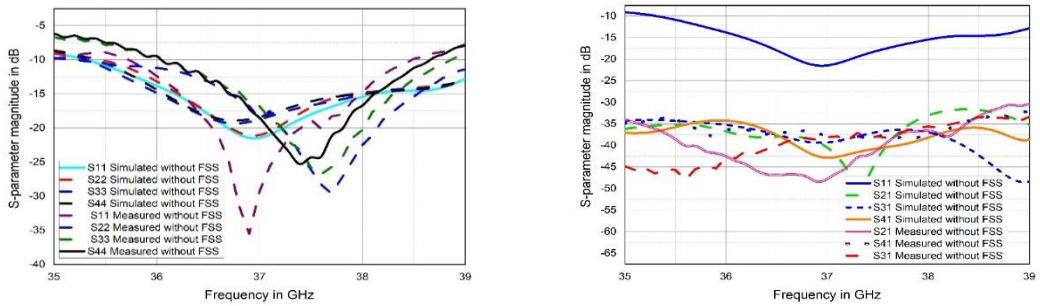

(c) (d)

Figure 25. Simulated and measured S-parameters of the proposed MIMO antenna at mmWave band (a), (b) with FSS, (c), (d) without FSS.

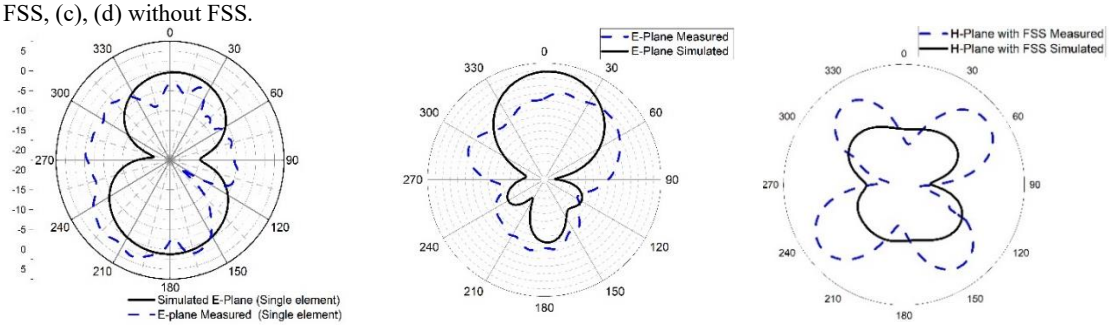

(a) (b) (c)

Figure 26. Radiation pattern measured and simulated values for single element antenna at sub-6; (a) without FSS, (b), (c) with FSS

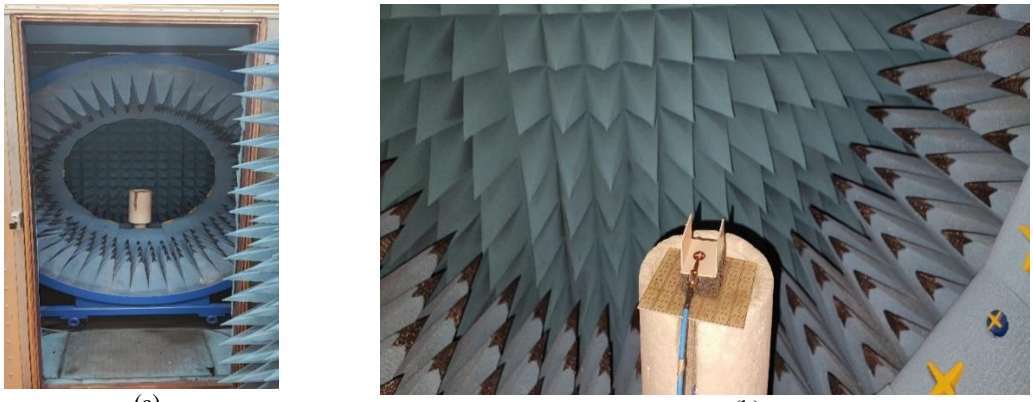

(a) (b)

Figure 27. Simulated and measured radiation pattern values for single element antenna (a) without FSS and (b) with FSS

5. Conclusion

Dual-band MIMO antennas for 5G base stations with impedance bandwidths of 1.5 and 3 GHz for sub-6 and mmWave bands, respectively, are achieved. The proposed MIMO antenna had a size of 82×76×1.524 mm^3 with isolation below -16.6 dB and -34 dB for both bands. A frequency-selective surface was used to enhance the MIMO system parameters; one was used underneath the patch for the sub-6 band, and another was vertically beside the patch for the mm-wave band. Gain improved from 1.8 to 8.7 dB at low frequency and 8.5 to 11.2 dB at high frequency. The suggested designs significantly improved the MIMO parameters, including ECC, DG, and TARC. The proposed antenna is tested in real-world coverage using Winprop software with Frankfurt as an urban area; the antenna proves coverage enhancement when using the FSS. Three sites with three sector antenna (single and 2×2 MIMO) are used. Using frequency selective surfaces data rates and throughput enhanced for single element working at sub-6 enhanced from 1.5 MB/s to 1.8 MB/s by 20%, and 150 MB/s to 187.7 MB/s by 25%, respectively in DL and UL when using FSS underneath the antenna and enhanced by 72% from 579.9 kB/s to 1.08 MB/s and throughput from 192 MB/s to 305.3 MB/s by 62% in mmWave frequency band when using FSS on single element's sides. Better references signal when applying FSS, RSRP enhanced in single

element from -90 dBm to -80 dBm in sub-6 band, from -94 dBm to -80 dBm in the mmWave band also in 2×2 MIMO it keeps excellent values > -80 dBm at both bands. RSRQ enhanced in 2×2 MIMO in both bands from -12 to -5 dB, RSSI results are all > -65 dBm, which is excellent in both bands.

References

[1] T. G. Abouelnaga, I. Zewail, and M. Shokair, "16-ports indoor base station MIMO array for sub-6 GHz 5G applications," *Telecommun Syst*, vol. 80, no. 4, pp. 589–597, 2022, doi: 10.1007/s11235-022-00916-z.

[2] T. Z. Fadhil, N. A. Murad, M. K. A. Rahim, M. R. Hamid, and L. O. Nur, "A Beam-Split Metasurface Antenna for 5G Applications," *IEEE Access*, vol. 10, pp. 1162–1174, 2022, doi: 10.1109/ACCESS.2021.3137324.

[3] Z. Duan, J. Rui, L. J. Xu, and G. Wen, "A low-profile dual-band dual-polarized tightly spaced antenna array with artificial magnetic conductor surface for 5G micro base station application," *Int. J. of RF and Microwave CAE*, vol. 32, no. 7, Jul. 2022, doi: 10.1002/mmce.23192.

[4] S. S. Al-Bawri, M. T. Islam, M. S. Islam, M. J. Singh, and H. Alsaif, "Massive metamaterial system-loaded MIMO antenna array for 5G base stations," *Sci Rep*, vol. 12, no. 1, Dec. 2022, doi: 10.1038/s41598-022-18329-y.

[5] A. Abdelaziz and E. K. I. Hamad, "Design of a Compact High Gain Microstrip Patch Antenna for Tri-Band 5G Wireless Communication," *Frequenz*, vol. 73, no. 1–2, pp. 45–52, Jan. 2019, doi: 10.1515/freq-2018-0058.

[6] X. Zhang and L. Zhu, "Gain-Enhanced Patch Antennas with Loading of Shorting Pins," *IEEE Trans Antennas Propag*, vol. 64, no. 8, pp. 3310–3318, Aug. 2016, doi: 10.1109/TAP.2016.2573860.

[7] M. Alyaboul-dahab, H. Hamed, M. Ghouz, A. Zakaria, and A. Zaki, "Tunable Microstrip Patch Antenna using FSS for WLAN Applications," *National Radio Science Conference*, 2016, pp. 64–72.

[8] Y. Zhang, X. Y. Zhang, L. H. Ye, and Y. M. Pan, "Dual-Band Base Station Array Using Filtering Antenna Elements for Mutual Coupling Suppression," *IEEE Trans Antennas Propag*, vol. 64, no. 8, pp. 3423–3430, Aug. 2016, doi: 10.1109/TAP.2016.2574872.

[9] W. Ali, S. Das, H. Medkour, and S. Lakrit, "Planar dual-band 27/39 GHz millimeter-wave MIMO antenna for 5G applications," *Microsystem Technologies*, vol. 27, no. 1, pp. 283–292, 2021, doi: 10.1007/s00542-020-04951-1.

[10] Y. Zhu, Y. Chen, and S. Yang, "Integration of 5G Rectangular MIMO Antenna Array and GSM Antenna for Dual-Band Base Station Applications," *IEEE Access*, vol. 8, pp. 63175–63187, 2020, doi: 10.1109/ACCESS.2020.2984246.

[11] W. Wu, H. Peng, and J. Mao, "A New Compact Dual-Polarized Co-axial Full-Band Antenna for 2G/3G/LTE Base Station Applications," *IEEE Electrical Design of Advanced Packaging and Systems Symposium (EDAPS)*, pp. 1–3, Dec. 2017.

[12] A. Abdelaziz and E. K. I. Hamad, "Isolation enhancement of 5G multiple-input multiple-output microstrip patch antenna using metamaterials and the theory of characteristic modes," *International Journal of RF and Microwave Computer-Aided Engineering*, vol. 30, no. 11, Nov. 2020, doi: 10.1002/mmce.22416.

[13] M. S. Abdel-Fattah, E. K. I. Hamad, T. G. Aboulnaga, S. A. Khaleel, and H. A. Elsadek, "Compact UWB Microstrip Patch Antenna for 5G Mobile Handset Applications," *International Journal Of Microwave And Optical Technology*, vol. 18, no. 3, May 2023.

[14] S. Davis *et al.*, "Ericsson Mobility Report Letter from the publisher 5G standalone brings new opportunities," Sweden, Nov. 2023.

[15] Erik Dahlman, Stefan Parkvall, and Johan Skold, *5G NR the Next Generation Wireless Access Technology*, Second. India: Mara Conner, 2021.

[16] "Guidelines for evaluation of radio interface technologies for IMT-2020." [Online]. Available: http://www.itu.int/en/ITU-R/study-groups/rsg5/rwp5d/imt-2020/Pages/submission-eval.aspx

[17] A. Bellary, K. Kandasamy, and P. H. Rao, "Analysis of Wave Propagation Models with Radio Network Planning Using Dual Polarized MIMO Antenna for 5G Base Station Applications," *IEEE Access*, vol. 10, pp. 29183–29193, 2022, doi: 10.1109/ACCESS.2022.3158948.

[18] H. Zahra, W. A. Awan, W. A. E. Ali, N. Hussain, S. M. Abbas, and S. Mukhopadhyay, "A 28 GHz broadband helical inspired end-fire antenna and its mimo configuration for 5g pattern diversity applications," *Electronics*, vol. 10, no. 4, pp. 1–15, 2021, doi: 10.3390/electronics10040405.

[19] Syeda Iffat Naqvi, Niamat Hussain, and Amjad Iqbal, "Integrated LTE and millimeter-wave 5g mimo antenna system for 4G/5G wireless terminals," *Sensors*, vol. 20, no. 14, pp. 1–20, Jul. 2020, doi: 10.3390/s20143926.

[20] Receiver characteristics: 3GPP Ts 38.521, "3GPP TS 38.521," 2022.

[21] Technical Report: "3rd Generation Partnership Project (3GPP); Release 15, 2020. [Online]. Available: http://www.3gpp.org.